QCD radiation effects on the $H \rightarrow WW \rightarrow \ell\nu\ell\nu$ signal at the LHC

Charalampos Anastasiou, Günther Dissertori and Fabian Stöckli

Institute for Theoretical Physics, ETH Zurich,
8093 Zurich, Switzerland
E-mail: babis@phys.ethz.ch, dissertori@phys.ethz.ch, fabstoec@phys.ethz.ch

Bryan R. Webber

Cavendish Laboratory, Cambridge CB3 0HE, U.K.
E-mail: webber@hep.phy.cam.ac.uk

ABSTRACT: The discovery of a Standard Model Higgs boson is possible when experimental cuts are applied which increase the ratio of signal and background cross-sections. In this paper we study the pp $\rightarrow$ H $\rightarrow$ WW signal cross-section at the LHC which requires a selection of Higgs bosons with small transverse momentum. We compare predictions for the efficiency of the experimental cuts from a NNLO QCD calculation, a calculation of the resummation of logarithms in the transverse momentum of the Higgs boson at NNLL, and the event generator MC@NLO. We also investigate the impact of various jet-algorithms, the underlying event and hadronization on the signal cross-section.

Contents

1. Introduction

Physical processes at collider experiments can be simulated using flexible event generators such as PYTHIA [1] and HERWIG [2]. In this approach, the momenta of partons in hard scattering processes are distributed among hadrons using an approximate probabilistic algorithm for parton branching and hadronization. Traditionally, event generators compute the hard scattering partonic cross-section at leading order in fixed order perturbation theory which yields only a rough estimate.

Cross-sections for the hard interaction of three or four particles can be computed routinely through next-to-leading order (NLO) in the α_s expansion. The results from NLO QCD calculations and parton shower event generators are often combined with an empiric method. First the efficiency of the experimental cuts and normalized differential distributions are computed with parton shower event generators. Then, they are multiplied with the result for the total cross-section from the NLO calculation.[1] However, it is now understood how to combine parton shower generators and NLO results with theoretically sound methods so that (i) leading logarithms are resummed with the parton shower, and (ii) all differential cross-sections are exactly accurate through NLO upon an expansion of the Sudakov factors in α_s [5, 6].

Fixed order perturbative computations have now advanced beyond the next to leading order, and there are two hadron collider processes which are known through next-to-next-to-leading order (NNLO) in α_s. The NNLO total cross-section of the Drell-Yan process [7, 8] is the most precise theoretical prediction for a hadron collider observable with a scale variation uncertainty of about 1%. The total cross-section for Higgs boson production is also known at NNLO [8–12]. For the LHC, the NLO [13, 14] and NNLO corrections are both important and increase the LO result by about 70% and 30% respectively. The

---

[1]Note that differential "K-factors" to reproduce bin integrated differential distributions at higher orders in perturbation theory are also used [3, 4].

perturbative series converges slowly and the remaining theoretical uncertainty is about ±10% [15, 8 – 12].

In Higgs boson [16 – 18] and electroweak gauge boson [19 – 22] production there exist novel differential cross-section calculations at NNLO [16, 17, 19 – 22, 18].[2] The cross-sections with arbitrary experimental cuts applied at the parton level can be computed exactly at this order in perturbation theory for the two processes. It is very instructive to compare the efficiencies of experimental cuts from the newly available fully differential NNLO calculations, merged NLO and parton-shower calculations with MC@NLO, and simple leading order event generators. This is valuable in order to estimate the inherent theoretical uncertainties of the above approaches.

Such a comparison can be made for the Drell-Yan process with the results from refs. [21, 22, 26], as well as discussed in ref. [21]. MC@NLO and the NNLO Monte-Carlo FEWZ [21, 22] predict very similar experimental efficiencies for the entire kinematic range where the NNLO prediction retains its phenomenal scale variation of about 1%. Significant differences, however, arise when the experimental cuts suppress contributions from the two-loop matrix elements.

A similar comparison [27] between MC@NLO and the NNLO partonic Monte-Carlo FEHiP has been made for the Higgs boson diphoton signal at the LHC. The signal cross-section is known with a scale uncertainty of about ±7% at NNLO [17]. Besides a relatively large perturbative correction from NLO to NNLO of about 20%, the efficiency of the experimental cuts turns out to be very similar in MC@NLO and NNLO [27].

A challenging channel for the Higgs boson discovery at the LHC is pp → H → WW. This channel is contaminated by background processes, pp → t$\bar{\text{t}}$ and pp → WW, with much larger cross-sections. For a Higgs boson with a mass close to the W-pair threshold, the cross-sections for all other discovery signals are suppressed. In this case, the pp → H → WW → ℓνℓν process becomes the only viable channel for the Higgs boson to be discovered at the LHC. It is thus indispensable to achieve a very good signal to background (S/B) ratio. An optimized selection of W-pair events [28] is then required. If appropriate cuts are applied, as in refs. [29 – 32], a discovery of a Standard Model Higgs boson with a mass close to the threshold should be achieved with an integrated luminosity of a few fb^{-1} at the LHC.

The pp → H → WW → ℓνℓν decay mode was recently implemented in the NNLO Monte-Carlo FEHiP [17] and a calculation of the cross-section with the experimental cuts of ref. [29, 30] was performed in ref. [33]. The very good agreement of the MC@NLO and NNLO calculations for the efficiency of the experimental cuts in the diphoton signal [27, 17, 5] does not guarantee that a similarly good agreement will be found in the H → WW channel. In this paper, we will compare the NNLO predictions from ref. [33] with resummation calculations and event generators.

In the H → γγ channel, the experimental cuts select events "democratically", irrespectively of the transverse momentum of the jets associated with the Higgs boson production.

---

[2]In non-hadronic collisions the state of the art at NNLO is fully differential cross-sections for $e^+e^- \to$ 3 jets [23 – 25].

The event selection in the H $\to$ WW channel [30, 31] imposes an explicit jet-veto and other cuts which reject events with large transverse momentum $p_{\mathrm{T}}^{\mathrm{H}}$ for the Higgs boson. This may turn out to be problematic for an agreement in experimental efficiencies between MC@NLO and NNLO for two reasons. First, the NNLO/NLO K-factor is sensitive to the cutoffs imposed on the $p_{\mathrm{T}}^{\mathrm{H}}$ [34, 16, 17]; this effect is treated only in the parton shower approximation in MC@NLO. Second, by selecting events with low $p_{\mathrm{T}}^{\mathrm{H}}$, multiple gluon radiation effects which are not included in the fixed order NNLO calculation may be important.

The resummation through next-to-next-to-leading logarithms (NNLL) of $p_{\mathrm{T}}^{\mathrm{H}}$ is now achieved [35 – 37]. The resummed spectrum, after matching to fixed order, integrates to the NNLO total cross-section. This calculation takes into account consistently both multiple gluon radiation effects at low transverse momentum and fixed order high transverse momentum contributions.

A theoretical prediction for the signal cross-section pp $\to$ H $\to$ WW $\to \ell\nu\ell\nu$ cannot be made directly from the $p_{\mathrm{T}}^{\mathrm{H}}$ spectrum, since the experimental cuts restrict many phase-space variables. The cross-section must therefore be computed using fully differential Monte-Carlo programs. However, we will use the resummation calculation of the $p_{\mathrm{T}}^{\mathrm{H}}$ spectrum [38, 36, 37] to validate fixed order Monte-Carlo's and parton shower event generators in the low $p_{\mathrm{T}}^{\mathrm{H}}$ kinematic region, which is favored by the experimental selection cuts.

We first compare in section 2 the theoretical calculations from the NNLL resummation [38], MC@NLO [5] and NNLO [33] for the $p_{\mathrm{T}}^{\mathrm{H}}$ spectrum. Then we compare in section 3 the MC@NLO [5], HERWIG [2] and NNLO [33] Monte-Carlo predictions for kinematic distributions of variables which are restricted by the experimental selection.[3] We perform a similar comparison for the signal cross-sections when all cuts are applied. We find a good agreement for the efficiencies of experimental cuts and normalized kinematic distributions. This gives us confidence that the selection of events for the signal cross-section does not invalidate the approximations in the used Monte-Carlo programs.

In section 4 we study the sensitivity of the signal cross-section with all experimental cuts applied to the choice of jet algorithm. We find a mild change on the cross-section ($\sim 6\%$) by using the SISCone or the k_{T}-algorithm. We also study the effect of hadronization (using the model in HERWIG [2]) and of the underlying event (using the JIMMY model [39]). We find that proposed experimental cuts render the cross-section sensitive to these effects at the level of up to $5 - 10\%$. The changes to the cross-section are with opposite signs and the combined effect is rather mild.

2. Integrating over the transverse momentum of the Higgs boson

In this section we compare fixed order [17] and parton shower calculations [2, 5] against the theoretical predictions for the transverse momentum spectrum of the Higgs boson from resummation [38]. Fixed order perturbation theory is invalid for small values of $p_{\mathrm{T}}^{\mathrm{H}}$. Nevertheless, observables can be reliably computed if their definition allows for an

---

[3]In the case of MC@NLO and HERWIG, we use a modified version of HERWIG with the correct decay angular correlations.
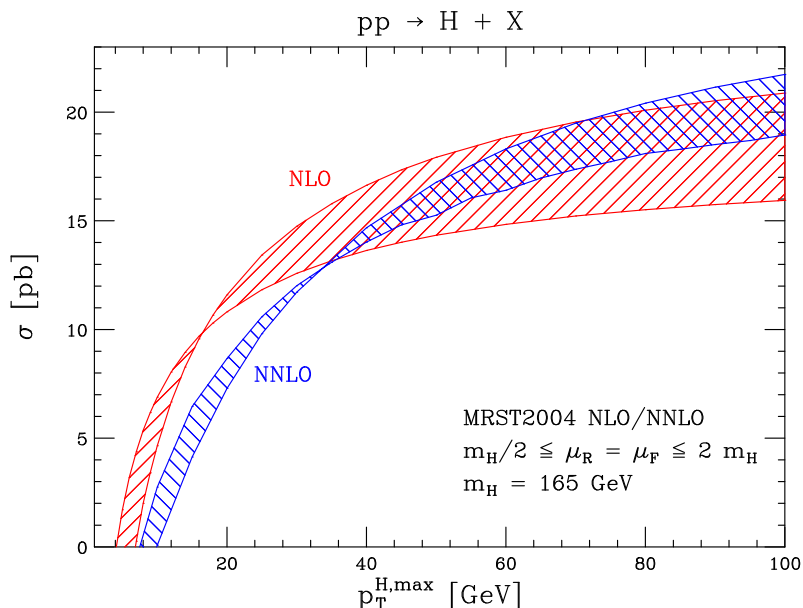
Figure 1: Cumulative cross-section for the Higgs transverse momentum distribution at fixed NLO and NNLO α_s expansion.

integration over a sufficiently large range in p_T^H values. Here, we study the cumulative cross-section

$$\sigma(p_T^{H,max}) = \int\limits_0^{p_T^{H,max}} \frac{\partial \sigma}{\partial p_T^H} \, dp_T^H \,. \tag{2.1}$$

This observable mimics the effect of selection cuts with a cutoff on the maximum Higgs transverse momentum. Since in the transverse plane the Higgs boson balances the associated jet radiation, the cross-section with a jet-veto is similar to the cross-section with a veto on high values of p_T^H.

In figure 1 we plot the cross-section in the fixed NLO and NNLO α_s expansion. As in all plots of this paper, we show the scale variation in the interval $m_H/2 < \mu_F = \mu_R < 2m_H$. The fixed order cross-sections at NLO and NNLO become negative and tend to infinity when the p_T^H cutoff is small (below $10\,\text{GeV}$). For such small values of $p_T^{H,max}$ perturbation theory breaks down. We observe that for larger cutoffs (above $40\,\text{GeV}$ and up to $100\,\text{GeV}$) the NLO and NNLO results are in very good agreement. The NNLO cross-section increases however faster than NLO with higher cutoffs leading to the known by $\sim 20\%$ larger NNLO result with respect to NLO for the total cross-section [8–10]. The analyses in ref. [29, 30] show that a better S/B ratio is achieved if stricter than 40 GeV cutoffs are used for the jet transverse momenta; for cutoff values in between $20\,\text{GeV}$ and $40\,\text{GeV}$ we observe large perturbative corrections.

In figure 2 we compare the fixed NLO result with the resummed NLL p_T^H spectrum from ref. [38] and with MC@NLO [5] without hadronization and underlying event. We find that
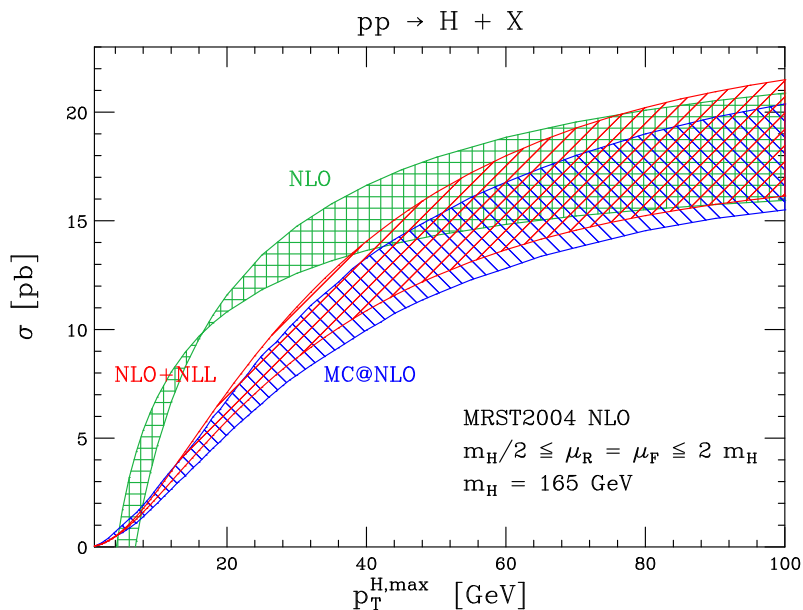
Figure 2: Cumulative cross-section for the Higgs transverse momentum distribution with MC@NLO, NLL resummation [38] and at NLO.

for $p_T^H < 40$ GeV the parton shower or the NLL resummation change significantly the integrated NLO p_T^H distribution. All results converge for higher and higher cutoffs $p_T^{H,max}$ and agree with each other for the fully inclusive cross-section. Notably, the MC@NLO and the NLL resummation are in a rather good agreement with each other within the uncertainties from scale variation.

Differences between cross-section predictions with fixed order perturbation theory and resummation are expected to become smaller when the fixed order calculations are extended to higher orders.

In [33] it was found that the average p_T^H of the Higgs boson, when discovery selection cuts are applied, can be as low as $< p_T^H > \simeq 15$ GeV. This leads to the question whether the NNLO result, unlike the NLO result, is a reliable prediction for such small values of the average p_T^H. In figure 3 we compare the integrated p_T^H distribution at NNLO against the resummed NNLL spectrum. We find a very good agreement between the two approaches for surprisingly low values of $p_T^{H,max}$. We conclude that higher than NNLO perturbative contributions, which are accounted for with the resummation, remain small for the integrated p_T^H spectrum, when the maximum Higgs transverse momentum is restricted even down to 20 GeV.

We have now validated the NNLO perturbative calculation [33] in a challenging case for fixed order perturbation theory which similarly emerges, due to the jet-veto and other cuts favoring small p_T^H values, in the search for a Higgs boson in the WW decay channel. However, the simulation of processes at NNLO is only performed at the parton level. We would like to investigate whether parton shower Monte-Carlo programs, which can also
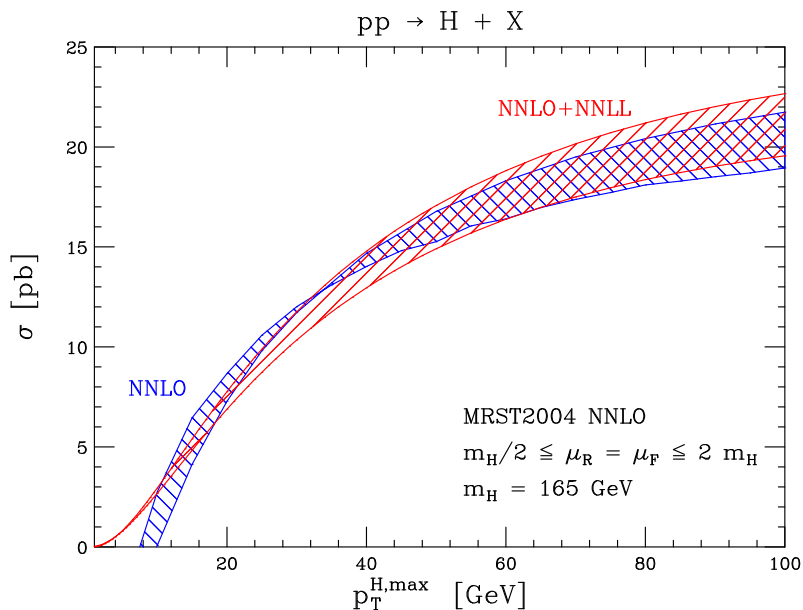
Figure 3: Cumulative cross-section for the Higgs transverse momentum distribution at NNLO in fixed order and with NNLL resummation [38]. The two approaches agree very well in the kinematic range which is relevant for the envisaged experimental cuts.

model non-perturbative effects and are computationally more flexible than NNLO Monte-Carlo's, provide realistic estimates of the signal cross-section.

We first discuss the problem of the normalization of the event generators. Parton shower Monte-Carlo programs predict the same total cross-section as the cross-section for their encoded partonic hard scattering at fixed order in perturbation theory. Therefore, HERWIG predicts the Higgs boson total cross-section with LO accuracy (underestimating it by a factor of ~ 2) and MC@NLO provides NLO precision (underestimating the total cross-section by a factor of ~ 1.25). A matching of parton showers to NNLO fixed order calculations is not yet developed. Following a practical approach, we will validate whether the efficiency of experimental cuts and normalized differential distributions are in agreement with the NNLO calculations of ref. [33]. We will then rescale the predictions of the MC@NLO and HERWIG event generators with a global K-factor in order to reproduce the fixed order result for the total cross-section. We will denote that the results of the Monte-Carlo X have been multiplied with a K-factor using the notation $R(X)$.

Now we will test how well event generators agree with resummation results for the p_T^H spectrum. In figure 4 we compare the integrated p_T^H spectrum of MC@NLO and HERWIG against the resummed NNLL prediction. We observe that both generators are in very good agreement with the NNLL spectrum. This is especially surprising for HERWIG which aims to describe the salient physics features of the process. Note, however, that MC@NLO gives slightly larger and HERWIG slightly smaller values than the NNLL resummation [38].
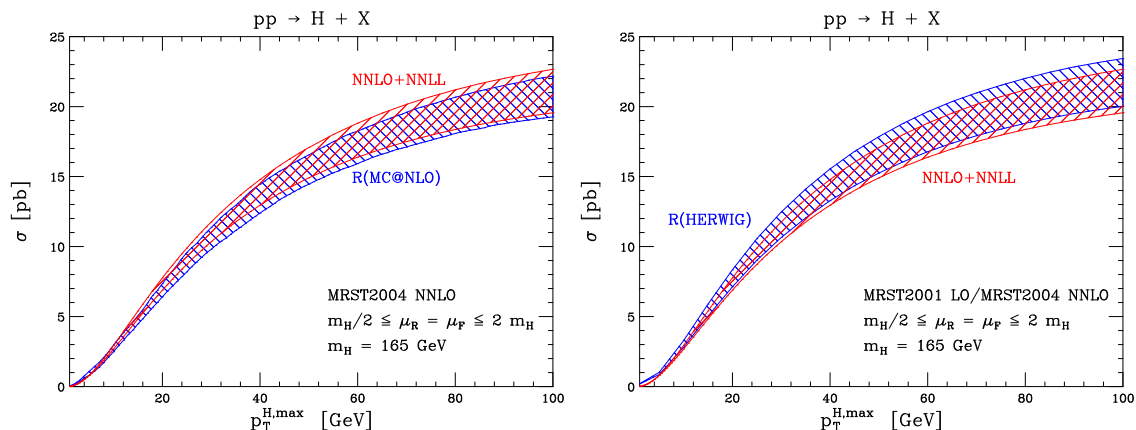
Figure 4: Cumulative cross-section for the Higgs transverse momentum distribution. The scaled MC@NLO and HERWIG spectra agree very well with the resummed NNLL spectrum [38].

σ $[pb]$	$\mu_R = \frac{m_{\mathrm{H}}}{4}$	$\mu_R = \frac{m_{\mathrm{H}}}{2}$	$\mu_R = m_{\mathrm{H}}$	$\mu_R = 2m_{\mathrm{H}}$
$\mu_F = \frac{m_{\mathrm{H}}}{4}$	13.31 ± 0.13	13.76 ± 0.08	13.45 ± 0.05	12.82 ± 0.04
$\mu_F = \frac{m_{\mathrm{H}}}{2}$	13.15 ± 0.13	13.85 ± 0.08	13.69 ± 0.06	13.14 ± 0.04
$\mu_F = m_{\mathrm{H}}$	13.13 ± 0.13	14.00 ± 0.08	13.96 ± 0.06	13.47 ± 0.04
$\mu_F = 2m_{\mathrm{H}}$	13.05 ± 0.13	14.15 ± 0.08	14.21 ± 0.06	13.76 ± 0.04

Table 1: The cross-section at NNLO for $p_T^{H,max} = 37 GeV$, varying independently the renormalization and factorization scales. The errors correspond to the numerical integration.

Before we conclude our analysis of the integrated $p_{\mathrm{T}}^{\mathrm{H}}$ distribution we wish to comment further on the scale variation of the fixed order results. In figure 1 we find a $p_{\mathrm{T}}^{\mathrm{H,max}}$ with no scale variation. A similar behavior is also observed for the accepted cross-section with all experimental cuts [29, 30] in ref. [33]. It is therefore necessary to investigate in better detail the variation of the NNLO result. We show the value of the cross-section at NNLO for $p_{\mathrm{T}}^{\mathrm{H,max}} \simeq 37\,\mathrm{GeV}$ (table 1), varying independently the renormalization and factorization scales (the errors correspond to the numerical integration). The cross-section is more sensitive to independent variations of the renormalization and factorization scales; however, this variation is significantly smaller than in the total cross-section. A detailed study of the cross-section when all experimental discovery cuts are applied, which shows a similar scale-variation pattern, has been made in ref. [33].

Summarizing, in this section we found that the integrated $p_{\mathrm{T}}^{\mathrm{H}}$ spectrum is predicted reliably at NNLO for the kinematic range of $p_{\mathrm{T}}^{\mathrm{H}}$ which is relevant in the search pp $\to$ H $\to$ WW $\to \ell\nu\ell\nu$. On the contrary, the NLO fixed order calculation is unreliable. We have also established that for the same observable, MC@NLO and HERWIG are in a very good agreement with the resummed NNLL spectrum when they are normalized to a common NNLO total cross-section.
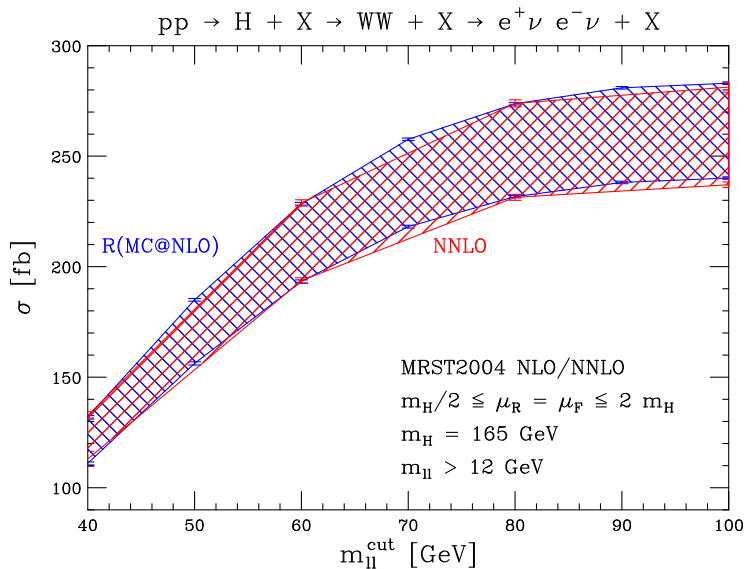
Figure 5: Cross-section when the lepton invariant mass is constrained in the interval $[12\,\text{GeV}, m_{\ell\ell}^{\text{cut}}]$ at NNLO and with MC@NLO.

3. Kinematic distributions and signal cross-section

The main backgrounds for the $pp \rightarrow H \rightarrow WW \rightarrow \ell\nu\ell\nu$ process are $pp \rightarrow t\bar{t}$ and $pp \rightarrow WW$. These backgrounds are sufficiently suppressed to allow for the discovery of a Higgs boson with a combination of experimental cuts [29, 30], exploiting the spin-correlations in the decay of the Higgs boson and the high average transverse momentum of jets in top-pair events. In ref. [33], the signal cross-section with these cuts was computed at NNLO. In this section we will compare the NNLO results of ref. [33] with MC@NLO. The public version of MC@NLO includes only partial spin-correlations for the $H \rightarrow WW \rightarrow \ell\nu\ell\nu$ decay. Here, the full spin-correlations for the decay of the Higgs boson have been implemented in MC@NLO. All the results of this paper correspond to a Standard Model Higgs boson mass of $m_{\text{H}} = 165\,\text{GeV}$.

In figures 5-8 we present the cross-sections when a single cut is applied on

- $m_{\ell\ell}$, the invariant mass of the charged lepton pair,

- $\phi_{\ell\ell}$, the angle between the two charged leptons in the plane transverse to the beam axis,

- $p_{\text{T,max}}^{\ell}$, the transverse momentum of the harder lepton, and

- $E_{\text{T}}^{\text{miss}}$, the missing transverse energy.

The four distributions show an excellent agreement for the efficiencies among NNLO and MC@NLO. This is a remarkable result and could not have been easily foreseen; there is a significant change in the shape of the $\phi_{\ell\ell}$, $p_{\text{T,max}}^{\ell}$, and $E_{\text{T}}^{\text{miss}}$ distributions from NLO to NNLO, as seen in ref. [33].

$$pp \rightarrow H + X \rightarrow WW + X \rightarrow e^+\nu \ e^-\nu + X$$

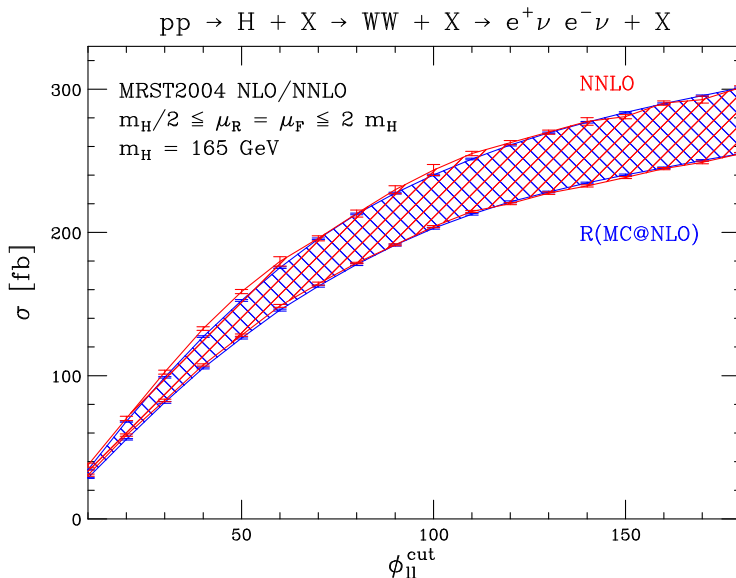**Figure 6:** Cross-section for the transverse opening angle of the two leptons in the interval $[0, \phi_{\ell\ell}^{\text{cut}}]$.

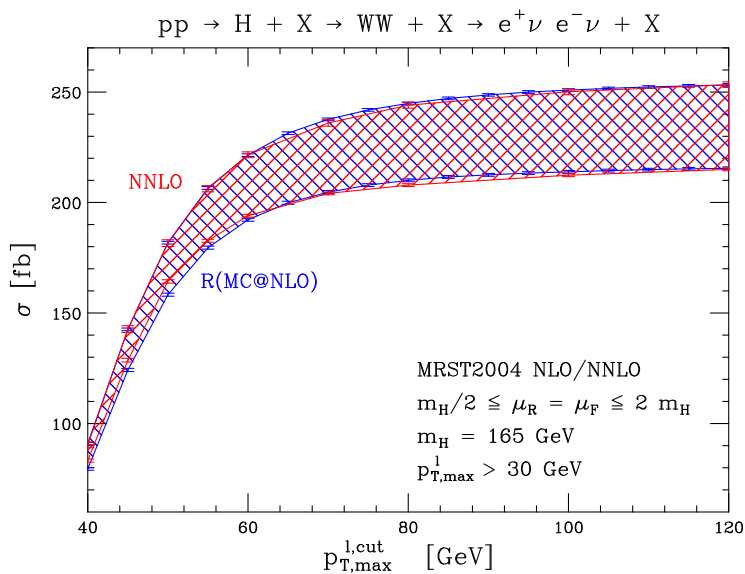$$pp \rightarrow H + X \rightarrow WW + X \rightarrow e^+\nu \ e^-\nu + X$$

Figure 7: Cross-section when the maximum transverse momentum of the leptons is in the range $\left[30 \, \text{GeV}, p_{\text{T,max}}^{\ell,\text{cut}}\right]$. Each lepton should have a transverse momentum of at least $25 \, \text{GeV}$.

A crucial experimental cut for suppressing the top-pair contribution to the background is a jet-veto. We veto events which have a transverse momentum of the leading jet in the central rapidity region ($|\eta_{\text{jet}}| < 2.5$) that is larger than $p_{\text{T}}^{\text{veto}}$. For the jet definition we use here a k_{T} algorithm with a jet-radius parameter $R = 0.4$; later we will also use a cone algorithm (SISCone [40]). The two algorithms are identical for the LO and NLO calculation
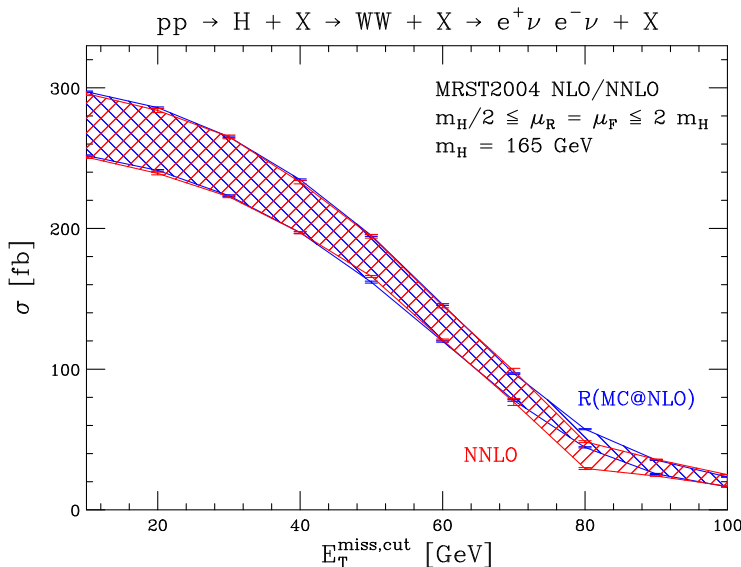
Figure 8: Cross-section when the missing transverse energy is $E_T^{miss} > E_T^{miss,cut}$.

where only up to one parton can be present in the final state, if the same jet-radius R is used. They differ, however, in the parton shower calculations (MC@NLO and HERWIG) and at NNLO as more partons are generated. In the envisaged experimental analysis a jet-veto with a rather small value of $p_T^{veto} \sim 25 - 40\,\text{GeV}$ is considered. We will investigate whether the NNLO and MC@NLO predictions are consistent with each other for such small values of the jet-veto.

The good agreement of the integrated p_T^H distribution between NNLO, MC@NLO and NNLL resummation suggests that a good agreement between MC@NLO and the NNLO cross-sections with a jet-veto may also hold. The jet-veto cross-section should be qualitatively similar to the cross-section with a cutoff on the p_T^H since at NLO the Higgs transverse momentum corresponds exactly to the transverse momentum of the additional jet. However, the two cuts are not exactly the same and they compare only qualitatively. The jet-veto applies only at central rapidities; in addition, beyond NLO the p_T^H is not the same variable as the maximum transverse momentum of the jets. In figure 9 we present the cross-section with a jet-veto applied. Indeed, we find a very good agreement between the NNLO result and MC@NLO (rescaled with the appropriate NNLO/NLO K-factor for the total cross-section).

In table 2 we list the cross-section after all *signal cuts* as described in ref. [33] are applied. We have used both the k_T and SISCone algorithm of ref. [40] and their implementation from ref. [41]. The jet radius in the azimuth-rapidity plane was set to $R = 0.4$ and the merging parameter for the SISCone algorithm to $f = 0.5$.[4] The two algorithms yield formally identical results for the fixed order calculation through NLO and indistinguish-

---

[4]The merging parameter f defines, how much two separate proto-jets need to overlap in order to be merged into one jet.

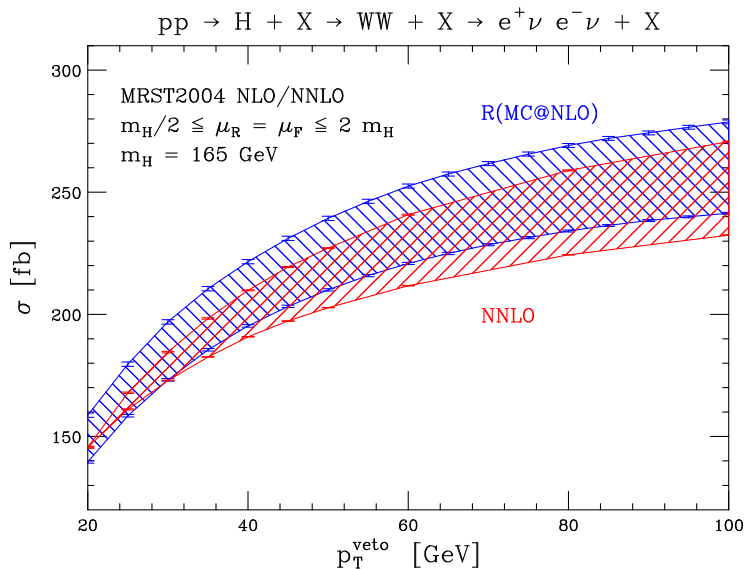**Figure 9:** The Higgs production cross-section with a fixed-order computation (NNLO) and MC@NLO rescaled with an inclusive K-factor (R(MC@NLO)) when a veto on jets with $p_T > p_T^{veto}$ at central rapidities $|\eta| < 2.5$ is applied.

able results at NNLO within our Monte-Carlo integration precision.[5] In the first section of the table we present the results obtained using a fixed-order LO computation and the LO+parton-shower event generator HERWIG. We find a much larger fixed order result than when a parton shower is added. At fixed leading order all events have a Higgs boson with zero transverse momentum, and the jet-veto rejects none of the events. On the contrary, HERWIG generates a large fraction of events with $p_T^{jet} > p_T^{veto}$.

In the second section of table 2 we present the results obtained using a fixed-order NLO computation, the event generator MC@NLO and HERWIG after we have rescaled it with an inclusive NLO/LO factor. While in MC@NLO and fixed order (LO, NLO and NNLO) we can set the renormalization and factorization scales for the hard scattering at will, we use HERWIG at the default scale since this affects the triggering of the hadronization procedure. We then rescale the HERWIG result using a K-factor, taking the NLO fixed order result to be at the scale $\mu = m_H/2$ or $\mu = 2m_H$. The NLO result is quite different from the one obtained with MC@NLO. We can attribute this failure of the NLO computation to the poor modeling of the low p_T region, as is shown in Fig 2.

In the last part of table 2 we present the results obtained using a fixed-order NNLO computation and the results from MC@NLO and HERWIG, rescaled to the NNLO total cross-section. The NNLO result and the rescaled MC@NLO give consistent results, albeit with different behavior when varying the renormalization and factorization scales. A detailed analysis of the NNLO scale dependence when all cuts are applied can be found in

---

[5]We thank Gavin Salam for pointing out to us that the SISCone and k_T algorithms are formally different already at NNLO.

$\sigma_{\rm acc}$ [fb]	$\mu = \frac{m_{\rm H}}{2}$		$\mu = 2\,m_{\rm H}$	
jet algorithm	SISCone	$k_{\rm T}$	SISCone	$k_{\rm T}$
LO	21.00 ± 0.02		14.53 ± 0.01	
HERWIG	11.16 ± 0.04	11.59 ± 0.04	7.60 ± 0.03	7.89 ± 0.03
NLO	22.40 ± 0.06		19.52 ± 0.05	
MC@NLO	17.42 ± 0.08	18.42 ± 0.08	13.60 ± 0.06	14.39 ± 0.06
$R^{\rm NLO}$(HERWIG)	19.79 ± 0.07	20.56 ± 0.07	14.61 ± 0.05	15.17 ± 0.05
NNLO	18.18 ± 0.43	18.45 ± 0.54	18.76 ± 0.31	19.01 ± 0.27
$R^{\rm NNLO}$(MC@NLO)	19.33 ± 0.09	20.43 ± 0.09	17.24 ± 0.07	18.24 ± 0.07
$R^{\rm NNLO}$(HERWIG)	22.02 ± 0.08	22.88 ± 0.08	18.65 ± 0.07	19.38 ± 0.07

Table 2: Cross-sections after the *signal cuts* of ref. [33] are applied for different calculation methods. The statistical integration errors are shown expicitly. The MC@NLO and HERWIG cross-sections are evaluated with 1,000,000 generated events. The fixed-order results were computed in ref. [33] and require the Monte-Carlo integration of multiple sectors [17].

ref. [33].

We note that for all the results of this section we use MC@NLO and HERWIG at the parton level, switching off the hadronization and without using a model for the underlying event. We observe that the $k_{\rm T}$-algorithm gives larger cross-sections than the SISCone algorithm for MC@NLO and HERWIG; as mentioned before, the results for the two algorithms are very similar at fixed order through NNLO (within our integration precision). Additionally MC@NLO gives slightly smaller values for the cross-sections than HERWIG.

We have established in this section that the efficiency of experimental cuts computed with MC@NLO and HERWIG is similar to the efficiency obtained at NNLO. There are rather dramatic changes in differential distributions when going from NLO to NNLO [33]. It is only at NNLO that the fixed order calculation is consistent with the parton shower efficiency of the experimental cuts. In the following section we will study the dependence of the cross-section on effects that are not captured by the fixed order NNLO calculation. We will study the effect of hadronization and of the underlying event. We will also investigate further the differences in the cross-section due to the two different jet algorithms.

4. Jet algorithms, hadronization and the underlying event

In this section we perform a study of the signal cross-section with all cuts applied using MC@NLO. We will analyze the impact of different jet clustering methods, hadronization and the underlying event.

In figure 10 we plot the cross-section using MC@NLO as a function of the $p_{\rm T}^{\rm veto}$ value for the $k_{\rm T}$ and the SISCone algorithm with a jet-radius $R = 0.4$ and $R = 0.7$. The clustering is applied to all final state particles before hadronization. We find that for small values of the jet-veto parameter the choice of the jet clustering method is more significant. For a jet-veto at $p_{\rm T}^{\rm veto} = 25\,{\rm GeV}$ the choice of jet-algorithm changes the cross-section by $\sim 6\%$ with MC@NLO. A similarly large variation of $\sim 7\%$ is observed when we vary the jet-
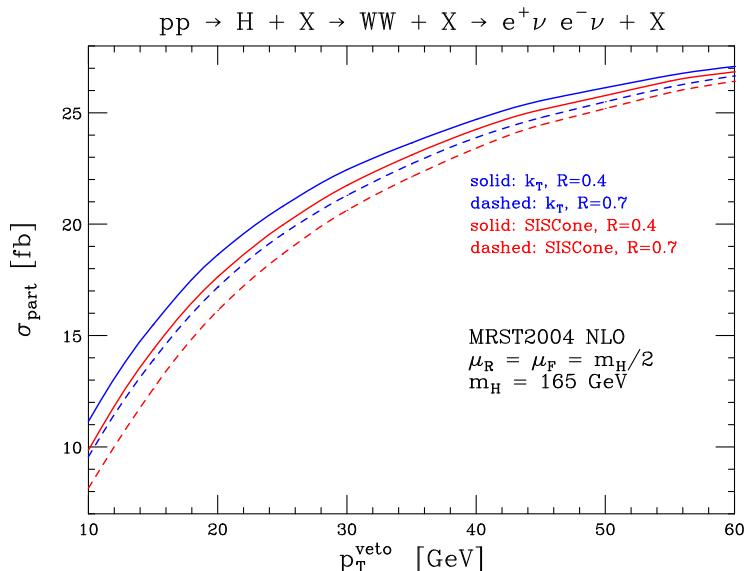
pp → H + X → WW + X → e⁺ν e⁻ν + X

solid: k_T, R=0.4
dashed: k_T, R=0.7
solid: SISCone, R=0.4
dashed: SISCone, R=0.7

MRST2004 NLO
$\mu_R = \mu_F = m_H/2$
$m_H = 165$ GeV

Figure 10: Comparison between the cone and k_T algorithm for different values of the allowed maximum jet transverse energy (jet-veto). All other cuts are set to the values chosen in ref. [33] for the *signal cuts.*
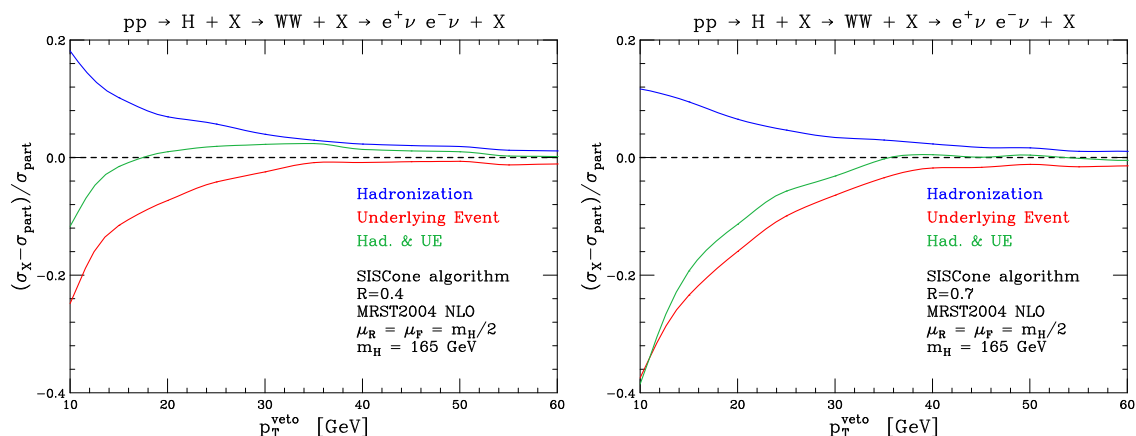

Figure 11: Difference of the cross-section after *signal cuts* including the underlying event and hadronization models, with respect to the partonic cross-section. The cross-section is shown as a function of the jet-veto value for the SISCone clustering algorithm.

radius from $R = 0.4$ to $R = 0.7$. For a jet veto value larger than about $p_T^{\text{veto}} \simeq 40\,\text{GeV}$ the sensitivity of the cross-section to the choice of the jet-algorithm or the jet-radius falls below $\sim 2-3\%$.

We now study the effect of hadronization as it is modeled in HERWIG and of the underlying event as implemented in JIMMY [39]. In figure 11 we present the relative difference of the cross-section with respect to the partonic cross-section when the hadronization or/and
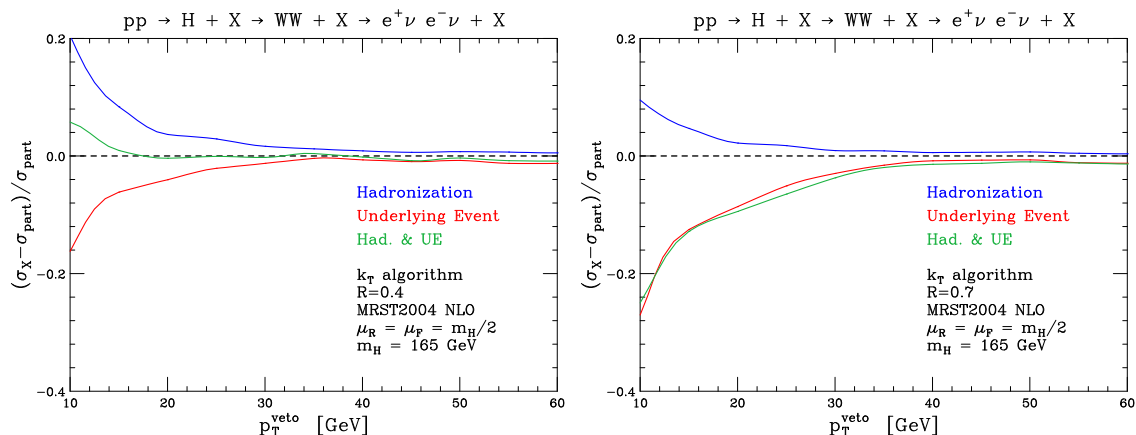
Figure 12: Difference of the cross-section after *signal cuts* including the underlying event and hadronization models, with respect to the partonic cross-section. The cross-section is shown as a function of the jet-veto value for the k_{T} clustering algorithm.

the underlying event models are switched on. We have used here the SISCone algorithm with a merging parameter $f = 0.5$ and two values for the jet-radius R=0.4 (left) and R=0.7 (right). We apply the *signal cuts* set to the values which are used in ref. [33]. We vary, however, the allowed maximum value of $p_{\mathrm{T}}^{\mathrm{jet}}$. Of interest are values of the jet-veto between 25 and 40 GeV, which are envisaged in the Higgs boson search.

Qualitatively, we anticipate that the hadronization and the underlying event change the partonic cross-section with opposite signs (we refer the reader to the recent analysis in ref. [42] for a detailed study). Hadronization reduces the average p_{T} of (gluonic) jets by roughly $\delta p_{\mathrm{T}} \sim (1\,\mathrm{GeV})/R$. The underlying event increases the jet p_{T} by roughly $\delta p_{\mathrm{T}} \sim R^2 \times (5\,\mathrm{GeV})$ at the LHC. The slope of the partonic cross-section with the jet-veto cutoffs (figure 9) is large for small values of the jet-veto. The shifts δp_{T} from hadronization and the underlying event can therefore induce significant changes to the cross-section. A jet-veto after hadronization corresponds to a looser effective jet-veto at the parton level. We therefore anticipate the cross-section to increase by switching on the hadronization model. Similarly, we anticipate a decrease of the cross-section due to the underlying event.

The trends can be verified in figure 11. A smaller jet-radius increases the impact of hadronization and decreases the impact of the underlying event. The two effects are not linearly additive. However, we find that a cancelation between the two effects, which varies according to the jet-radius, takes place. For a jet veto $p_{\mathrm{T}}^{\mathrm{veto}} = 25\,\mathrm{GeV}$ and a radius $R = 0.4$, the hadronization shift is about $\sim 7\%$ and the underlying event shift is $\sim 4\%$. For a larger radius $R = 0.7$, the two shifts are 5% and 10% correspondingly.

In figure 12 we show the effects of hadronization and the underlying event for the k_{T} algorithm. We find the same features qualitatively for the two effects as in the SISCone algorithm. We note however, that the k_{T}-algorithm shows an overall reduced sensitivity.

5. Conclusions

In this paper we have studied QCD effects for the process pp → H → WW → $\ell\nu\ell\nu$. This process is of particular interest at the LHC since it is possible that for a range of mass values of the Higgs boson, this channel is the only viable one for a discovery.

The cross-section with all envisaged experimental cuts applied was computed in an earlier publication [33] at NNLO in QCD. In this paper we compared these NNLO results with the leading order event generator HERWIG [2] and the event generator MC@NLO [5] which performs a matching of HERWIG with NLO fixed order perturbation theory. We found very good agreement in efficiencies of all experimental cuts that are relevant in the search for the Higgs boson. This is rather spectacular given that there are significant corrections in the total cross-section and the shape of kinematic distributions from NLO to NNLO.

The experimental cuts select events with small transverse momentum of the Higgs boson. This is important in order to reduce the selection of events from top-quark production, which is a major background. We have compared a NNLO computation and the result of NNLL resummation [38] for the cumulative p_T^H distribution. We found that NNLL resummation does not induce significant corrections with respect to the NNLO calculation for the kinematic range which is favoured by the selection cuts. We have also found that, within the uncertainty from scale variations, MC@NLO and HERWIG are in very good agreement with the NNLL result. On the contrary, fixed order NLO perturbation theory provides a rather poor approximation for the required distributions and efficiencies.

Finally, we investigated the magnitude of effects due to hadronization, the underlying event, and the choice of jet algorithms. For typical choices of parameters and cutoffs in the experimental cuts we find a mild dependence of the cross-section on these effects. In this paper we did not examine a variety of remaining uncertainties, such as uncertainties in the parton densities, which may be relevant at a precision level of 10%. Studies of electroweak corrections can be found in refs. [43–45] and of the background-signal interference in ref. [46].

The results and comparisons made in this paper provide a firm validation of the fixed order NNLO results and the event generator tools which are available for simulating the pp → H → WW → $\ell\nu\ell\nu$ process at the LHC.

References

[1] T. Sjostrand, S. Mrenna and P. Skands, *PYTHIA* 6.4 *physics and manual*, *JHEP* **05** (2006) 026 [hep-ph/0603175].

[2] G. Corcella et al., *HERWIG* 6*: an event generator for hadron emission reactions with interfering gluons (including supersymmetric processes)*, *JHEP* **01** (2001) 010 [hep-ph/0011363]; *HERWIG* 6.5 *release note*, hep-ph/0210213.

[3] G. Davatz, G. Dissertori, M. Dittmar, M. Grazzini and F. Pauss, *Effective K-factors for gg → H → WW → lνlν at the LHC*, *JHEP* **05** (2004) 009 [hep-ph/0402218].

[4] G. Davatz et al., *Combining Monte Carlo generators with next-to-next-to-leading order calculations: event reweighting for Higgs boson production at the LHC*, *JHEP* **07** (2006) 037 [hep-ph/0604077].

[5] S. Frixione and B.R. Webber, *Matching NLO QCD computations and parton shower simulations*, *JHEP* **06** (2002) 029 [hep-ph/0204244]; *The MC@NLO 3.3 event generator*, hep-ph/0612272.

[6] S. Frixione, P. Nason and B.R. Webber, *Matching NLO QCD and parton showers in heavy flavour production*, *JHEP* **08** (2003) 007 [hep-ph/0305252].

[7] R. Hamberg, W.L. van Neerven and T. Matsuura, *A Complete calculation of the order alpha-S^2 correction to the Drell-Yan K factor*, *Nucl. Phys.* **B 359** (1991) 343.

[8] R.V. Harlander and W.B. Kilgore, *Next-to-next-to-leading order Higgs production at hadron colliders*, *Phys. Rev. Lett.* **88** (2002) 201801 [hep-ph/0201206].

[9] C. Anastasiou and K. Melnikov, *Higgs boson production at hadron colliders in NNLO QCD*, *Nucl. Phys.* **B 646** (2002) 220 [hep-ph/0207004].

[10] C. Anastasiou and K. Melnikov, *Higgs boson production at hadron colliders in NNLO QCD*, *Nucl. Phys.* **B 646** (2002) 220 [hep-ph/0207004].

[11] R.V. Harlander and W.B. Kilgore, *Production of a pseudo-scalar Higgs boson at hadron colliders at next-to-next-to leading order*, *JHEP* **10** (2002) 017 [hep-ph/0208096].

[12] V. Ravindran, J. Smith and W.L. van Neerven, *NNLO corrections to the total cross section for Higgs boson production in hadron hadron collisions*, *Nucl. Phys.* **B 665** (2003) 325 [hep-ph/0302135].

[13] M. Spira, A. Djouadi, D. Graudenz and P.M. Zerwas, *Higgs boson production at the LHC*, *Nucl. Phys.* **B 453** (1995) 17 [hep-ph/9504378].

[14] S. Dawson, *Radiative corrections to Higgs boson production*, *Nucl. Phys.* **B 359** (1991) 283.

[15] C. Anastasiou, K. Melnikov and F. Petriello, *The gluon-fusion uncertainty in Higgs coupling extractions*, *Phys. Rev.* **D 72** (2005) 097302 [hep-ph/0509014].

[16] C. Anastasiou, K. Melnikov and F. Petriello, *Higgs boson production at hadron colliders: differential cross sections through next-to-next-to-leading order*, *Phys. Rev. Lett.* **93** (2004) 262002 [hep-ph/0409088].

[17] C. Anastasiou, K. Melnikov and F. Petriello, *Fully differential Higgs boson production and the di-photon signal through next-to-next-to-leading order*, *Nucl. Phys.* **B 724** (2005) 197 [hep-ph/0501130].

[18] S. Catani and M. Grazzini, *An NNLO subtraction formalism in hadron collisions and its application to Higgs boson production at the LHC*, *Phys. Rev. Lett.* **98** (2007) 222002 [hep-ph/0703012].

[19] C. Anastasiou, L.J. Dixon, K. Melnikov and F. Petriello, *Dilepton rapidity distribution in the Drell-Yan process at NNLO in QCD*, *Phys. Rev. Lett.* **91** (2003) 182002 [hep-ph/0306192].

[20] C. Anastasiou, L.J. Dixon, K. Melnikov and F. Petriello, *High-precision QCD at hadron colliders: electroweak gauge boson rapidity distributions at NNLO*, *Phys. Rev.* **D 69** (2004) 094008 [hep-ph/0312266].

[21] K. Melnikov and F. Petriello, *Electroweak gauge boson production at hadron colliders through $O(\alpha_s^2)$*, *Phys. Rev.* **D 74** (2006) 114017 [hep-ph/0609070].

[22] K. Melnikov and F. Petriello, *The W boson production cross section at the LHC through $O(\alpha_s^2)$*, *Phys. Rev. Lett.* **96** (2006) 231803 [hep-ph/0603182].

[23] A. Gehrmann-De Ridder, T. Gehrmann, E.W.N. Glover and G. Heinrich, *Second-order QCD corrections to the thrust distribution*, *Phys. Rev. Lett.* **99** (2007) 132002 [arXiv:0707.1285]; *Second-order QCD corrections to the thrust distribution*, *Phys. Rev. Lett.* **99** (2007) 132002 [arXiv:0707.1285].

[24] A. Gehrmann-De Ridder, T. Gehrmann, E.W.N. Glover and G. Heinrich, *Infrared structure of $e^+e^- \to 3$ jets at NNLO*, *JHEP* **11** (2007) 058 [arXiv:0710.0346].

[25] A. Gehrmann-De Ridder, T. Gehrmann, E.W.N. Glover and G. Heinrich, *NNLO corrections to event shapes in e^+e^- annihilation*, *JHEP* **12** (2007) 094 [arXiv:0711.4711].

[26] S. Frixione and M.L. Mangano, *How accurately can we measure the W cross section?*, *JHEP* **05** (2004) 056 [hep-ph/0405130].

[27] F. Stockli, A.G. Holzner and G. Dissertori, *Study of perturbative QCD predictions at next-to-leading order and beyond for $pp \to H \to \gamma\gamma + X$*, *JHEP* **10** (2005) 079 [hep-ph/0509130].

[28] M. Dittmar and H.K. Dreiner, *How to find a Higgs boson with a mass between $155\,GeV$ to $180\,GeV$ at the LHC*, *Phys. Rev.* **D 55** (1997) 167 [hep-ph/9608317].

[29] G. Davatz, M. Dittmar, A.-S. Giolo-Nicollerat, *Potential of CMS in the $H \to WW \to l\nu l\nu$ channel*, CMS Note 2006/047.

[30] G. Davatz, M. Dittmar and F. Pauss, *Simulation of a cross section and mass measurement of a SM Higgs boson in the $H \to WW \to lvlv$ channel at the LHC*, *Phys. Rev.* **D 76** (2007) 032001 [hep-ph/0612099].

[31] G. Davatz, M. Dittmar and A.S. Giolo-Nicollerat, *Standard model Higgs discovery potential of CMS in the $H \to WW \to l\nu l\nu$ channel*, *J. Phys.* **G 22** (2007) N85.

[32] G. Davatz, A. S. Giolo-Nicollerat and M. Zanetti, *Systematic uncertainties of the top background in the $H \to WW$ channel*, CERN-CMS-NOTE-2006-048.

[33] C. Anastasiou, G. Dissertori and F. Stockli, *NNLO QCD predictions for the $H \to WW \to ll\nu\nu$ signal at the LHC*, *JHEP* **09** (2007) 018 [arXiv:0707.2373].

[34] S. Catani, D. de Florian and M. Grazzini, *Direct Higgs production and jet veto at the Tevatron and the LHC in NNLO QCD*, *JHEP* **01** (2002) 015 [hep-ph/0111164].

[35] G. Bozzi, S. Catani, D. de Florian and M. Grazzini, *Higgs boson production at the LHC: transverse-momentum resummation and rapidity dependence, Nucl. Phys.* **B 791** (2008) 1 [arXiv:0705.3887].

[36] G. Bozzi, S. Catani, D. de Florian and M. Grazzini, *Transverse-momentum resummation and the spectrum of the Higgs boson at the LHC, Nucl. Phys.* **B 737** (2006) 73 [hep-ph/0508068].

[37] G. Bozzi, S. Catani, D. de Florian and M. Grazzini, *The q(T) spectrum of the Higgs boson at the LHC in QCD perturbation theory, Phys. Lett.* **B 564** (2003) 65 [hep-ph/0302104].

[38] G. Bozzi, S. Catani, D. de Florian and M. Grazzini, online at http://arturo.fi.infn.it/grazzini/codes.html.

[39] J.M. Butterworth, J.R. Forshaw and M.H. Seymour, *Multiparton interactions in photoproduction at HERA, Z. Physik* **C 72** (1996) 637 [hep-ph/9601371].

[40] G.P. Salam and G. Soyez, *A practical seedless infrared-safe cone jet algorithm, JHEP* **05** (2007) 086 [arXiv:0704.0292].

[41] M. Cacciari and G.P. Salam, *Dispelling the N^3 myth for the $K(t)$ jet-finder, Phys. Lett.* **B 641** (2006) 57 [hep-ph/0512210].

[42] M. Dasgupta, L. Magnea and G.P. Salam, *Non-perturbative QCD effects in jets at hadron colliders*, arXiv:0712.3014.

[43] G. Degrassi and F. Maltoni, *Two-loop electroweak corrections to Higgs production at hadron colliders, Phys. Lett.* **B 600** (2004) 255 [hep-ph/0407249].

[44] A. Bredenstein, A. Denner, S. Dittmaier and M.M. Weber, *Radiative corrections to the semileptonic and hadronic Higgs-boson decays $H \to WW/ZZ \to 4$ fermions, JHEP* **02** (2007) 080 [hep-ph/0611234].

[45] A. Bredenstein, A. Denner, S. Dittmaier and M.M. Weber, *Precise predictions for the Higgs-boson decay $H \to WW/ZZ \to 4$ leptons, Phys. Rev.* **D 74** (2006) 013004 [hep-ph/0604011].

[46] T. Binoth, M. Ciccolini, N. Kauer and M. Kramer, *Gluon-induced W-boson pair production at the LHC, JHEP* **12** (2006) 046 [hep-ph/0611170].